光学学报

间隔轨道角动量的复合涡旋光束编/解码

吴鹏飞[1*], 王小蝶[1], 王姣[2], 谭振坤[3], 贾致远[1]

[1]西安理工大学自动化与信息工程学院，陕西 西安 710048；

[2]陕西科技大学电子信息与人工智能学院， 陕西 西安 710021；

[3]西安工业大学光电工程学院，陕西 西安 710021

摘要 为提高传输系统的信道容量、编码效率以及解码的可靠性，本文提出了一种基于轨道角动量(OAM)模态和径向模态的复合涡旋光束编码方法。使用5位二进制序列对两束光[一束是具有固定径向模态和OAM模态的拉盖尔-高斯(LG)涡旋光束，另一束是具有4种径向模态(p=0,1,2,3)和8种相同间隔OAM模态(l=±3,±5,±7,±9)的LG涡旋光束]叠加产生的32组不同类型的复合涡旋光束光强分布图进行编码。将32组复合涡旋光束依据本文提出的映射关系转换成32组单束LG涡旋光束，依次照射在提出的x、y轴方向周期渐变光栅上，通过光栅的远场衍射光斑可成功检测出发射单束LG涡旋光束的参数p和l，且不受OAM模态和径向模态增加的影响，最终可实现正确解码。

关键词 物理光学；复合涡旋光束；轨道角动量；径向模态；周期渐变光栅；远场衍射光斑

中图分类号 P427.1 **文献标志码** A **DOI**: 10.3788/AOS222187

1 引 言

利用光的维度将数字信号进行编码是光通信的重要基础，传统的编码依赖于光的振幅、频率、相位、时间和极化等维度[1-3]，已经不能满足人们对大信道容量通信系统的需求。为了提高通信系统的信道容量和传输速率，1992年，Allen等[4]在电磁波领域证明了具有连续螺旋相位因子的涡旋光束存在相位奇点且携带轨道角动量(OAM)。涡旋光束因其独特的光场结构，使得它在量子信息处理[5-7]、生物医学[8]、光学处理[9]、天体探测[10]等领域得到了广泛的应用，特别是在空间光通信领域具有潜在的应用价值。

常见的涡旋光束有以下3种：拉盖尔-高斯光束、贝塞尔-高斯光束以及厄米高斯光束[11-13]。拉盖尔-高斯(Laguerre-Gaussian，LG)光束是一种典型的涡旋光束，可记为LG_p^l，其中，l为OAM模态(也称拓扑荷数)，p为径向模态。不同OAM模态的正交性以及OAM取值的多样性[14]，使得涡旋光束的编码技术成为目前光通信领域研究的热点之一。2014年，Anguita等[15]研究了两束LG光束的共轴叠加，极大地提高了信道容量，但所采用的LG光束的径向模态p均为0。2020年，He等[16]提出一种利用光学亮环晶格对空间光信息进行编码通信的方法。2021年，Nan等[17]利用两路多进制信号产生具有不同OAM值的涡旋光束再进行相干叠加，产生16种不同的光强图案，并提出了一种基于光强相关性的编码方案。2021年，Wang等[18]利用6位二进制序列对16种OAM模态(l=±1～±8)和4种径向模态(p=0～3)组成的64种涡旋光束进行编码，并且验证了编码在实践中的可行性和有效性。上述编码方式主要集中在单一的OAM模态或连续变化的OAM模态相互叠加，该编码方式在接收端解码时相邻的两个光束容易混淆，使得解码的可靠性降低。为了提高解码的可靠性，本文提出了一种基于OAM模态和径向模态的间隔型编码方式。

在接收端解码时，则需预先检测出涡旋光束的参数p和l。常见的涡旋光束检测方法有：扭矩测量法[19]、杨氏双缝干涉法[20]、衍射测量法(例如：环形光栅、复合叉形光栅、达曼涡旋光栅)[21-23]等。2006年，Sztul等[24]进行了涡旋光束的杨氏双缝干涉实验测量涡旋光束的OAM值。2010年，Zhang等[23]提出了一种新型的达曼涡旋光栅，可将OAM模态的连续可探测范围拓展至−12～+12，但其探测范围仍无法满足部分光通信的应用要求。2016年，Fu等[25]研究了一种可以检测多路OAM模态的光栅，主要是通过将5×5达曼涡旋光栅和阶数为+12或−12的螺旋相位板结合，使得OAM模态的探测范围扩展至−24～24，其适

收稿日期：2022-12-29；**修回日期**：2023-02-04；**录用日期**：2023-02-20；**网络首发日期**：2023-03-09

基金项目：陕西省教育厅服务地方专项计划项目(20JC027)、西安市高校院所科技人员服务企业项目(22GXFW0074)、国家自然科学基金(62001363，62101313)、陕西省科技厅重点研发计划-工业领域一般项目(2022GY-100)

通信作者：*wupengf@xaut.edu.cn

用于多个涡旋光束检测。2020年，Dedo等[26]提出并实验验证了一种基于格希伯格-萨克斯顿算法和卷积神经网络的联合方案，对OAM模态进行了精确识别。2021年，Wang等[27]研究了一种光学衍射神经网络的OAM模态逻辑运算法，通过各种逻辑门结构可反解出OAM模态。2022年，Fang等[28]研究了基于多相平面光转换的OAM模态解复用技术，通过相剖面图螺旋条纹信息，可一一对应地解出OAM值。但上述方法均是检测涡旋光束的OAM模态l，且目前对于径向模态p的检测偏少，因此本文提出基于周期渐变光栅，实现检测径向模态这一个参数。

本文提出一种基于OAM模态和径向模态的新型间隔编码方式，采用$LG_{p_1=0}^{l_1=2}$与$LG_{p_2}^{l_2}\{p_2=0,1,2,3;\ l_2=3,5,7,9\}$、$LG_{p_1=0}^{l_1=6}$与$LG_{p_2}^{l_2}\{p_2=0,1,2,3;l_2=-3,-5,-7,-9\}$进行共轴叠加，可以组成32组不同光强分布的复合涡旋光束，并用5位二进制序列对其进行编码。将32组复合涡旋光束依据本文提出的映射关系转换成32组单束LG涡旋光束，依次照射在提出的周期渐变光栅上，通过光栅的远场衍射可检测出入射光束的参数p和l，最终成功实现解码。

2 基础理论

LG涡旋光束沿z轴传播，其复振幅表达式为亥姆霍兹方程的解[29]，可表示为

$$E_p^l(r,\theta,z)=\sqrt{\frac{2p!}{\pi(p+|l|)!}}\times\frac{1}{\omega(z)}\times\left[\frac{\sqrt{2}\,r}{\omega(z)}\right]^{|l|}\times\exp\left[\frac{-r^2}{\omega^2(z)}\right]\times L_p^{|l|}\left[\frac{2r^2}{\omega^2(z)}\right]\times$$
$$\exp(-\mathrm{i}l\theta)\times\exp\left[\frac{-\mathrm{i}kr^2z}{2(z^2+z_R^2)}\right]\times\exp\left[\mathrm{i}(2p+|l|+1)\tan^{-1}\left(\frac{z}{z_R}\right)\right],\quad(1)$$

式中：θ为柱坐标下的方位角；z为传输距离；$\omega(z)=\omega_0\sqrt{1+(z/z_R)^2}$为光斑尺寸，其中，$\omega_0$为$z=0$时的束腰半径；$L_p^{|l|}[\cdot]$为拉盖尔多项式，当$p=0$时，$L_p^{|l|}[\cdot]=1$；$k=2\pi/\lambda$为波矢；$z_R=\pi\omega_0^2/\lambda$为瑞利长度；$(2p+|l|+1)\cdot\tan^{-1}(z/z_R)$为古伊相位。

当任意两个LG涡旋光束共轴叠加时，叠加后的复合涡旋光束强度表达式为

$$I=\left|E_f(r,\theta,z)\right|^2=(E_{p_1}^{l_1}+E_{p_2}^{l_2}).*\mathrm{conj}(E_{p_1}^{l_1}+E_{p_2}^{l_2})。\quad(2)$$

本文选取$LG_{p_1=0}^{l_1=2}$与$LG_{p_2}^{l_2}\{p_2=0,1,2,3;\ l_2=3,5,7,9\}$、$LG_{p_1=0}^{l_1=6}$与$LG_{p_2}^{l_2}\{p_2=0,1,2,3;\ l_2=-3,-5,-7,-9\}$进行叠加，可以得到32组叠加后的复合涡旋光束光强图，如图1所示。

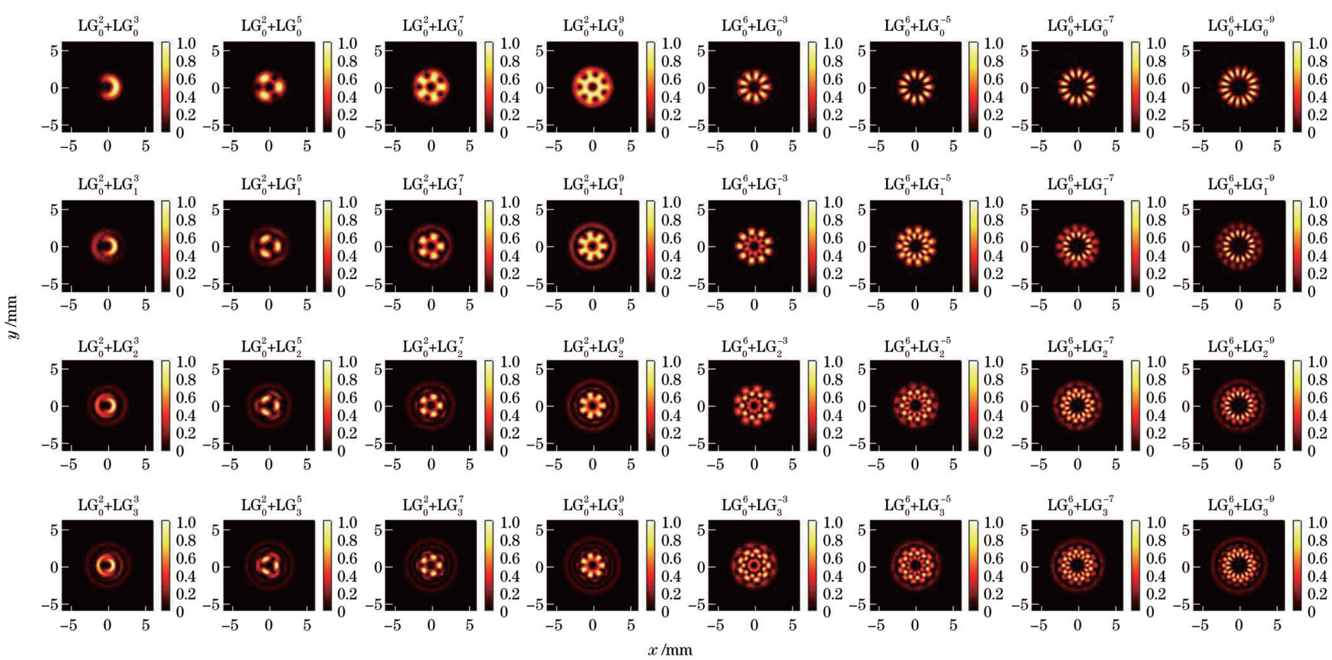

图1　32组复合涡旋光束光强分布图

Fig. 1　Intensity distributions of 32 composite vortex beams

由图1可以看出，光强图呈现明亮的多环状光斑。随着OAM模态$|l_2|$的增加，光强图各环的半径也逐渐增大，且每环的光斑数目均为$|l_2-l_1|$；随着径向模态p_2的增加，光强图的环数也逐渐增加，且环数为$p=\max(p_1,p_2)+1$。例如，复合涡旋光束$LG_0^2+LG_1^7$能被描述为2环5光斑。

3　编码原理

用5位二进制序列（00000～11111）对图1的32组复合涡旋光束光强分布图（$LG_0^2+LG_0^3$～$LG_0^6+LG_3^{-9}$）进行编码，编码结果见图2。

LG beam superposition		radial mode							
		$p=3$	sequence	$p=2$	sequence	$p=1$	sequence	$p=0$	sequence
OAM mode	$l=3$	$LG_0^2+LG_3^3$	11000	$LG_0^2+LG_2^3$	10000	$LG_0^2+LG_1^3$	01000	$LG_0^2+LG_0^3$	00000
	$l=5$	$LG_0^2+LG_3^5$	11001	$LG_0^2+LG_2^5$	10001	$LG_0^2+LG_1^5$	01001	$LG_0^2+LG_0^5$	00001
	$l=7$	$LG_0^2+LG_3^7$	11010	$LG_0^2+LG_2^7$	10010	$LG_0^2+LG_1^7$	01010	$LG_0^2+LG_0^7$	00010
	$l=9$	$LG_0^2+LG_3^9$	11011	$LG_0^2+LG_2^9$	10011	$LG_0^2+LG_1^9$	01011	$LG_0^2+LG_0^9$	00011
	$l=-3$	$LG_0^6+LG_3^{-3}$	11100	$LG_0^6+LG_2^{-3}$	10100	$LG_0^6+LG_1^{-3}$	01100	$LG_0^6+LG_0^{-3}$	00100
	$l=-5$	$LG_0^6+LG_3^{-5}$	11101	$LG_0^6+LG_2^{-5}$	10101	$LG_0^6+LG_1^{-5}$	01101	$LG_0^6+LG_0^{-5}$	00101
	$l=-7$	$LG_0^6+LG_3^{-7}$	11110	$LG_0^6+LG_2^{-7}$	10110	$LG_0^6+LG_1^{-7}$	01110	$LG_0^6+LG_0^{-7}$	00110
	$l=-9$	$LG_0^6+LG_3^{-9}$	11111	$LG_0^6+LG_2^{-9}$	10111	$LG_0^6+LG_1^{-9}$	01111	$LG_0^6+LG_0^{-9}$	00111

图2　32组复合涡旋光束对应的编码表

Fig. 2　Encoding table corresponding to 32 composite vortex beams

由图2可知，$LG_0^2+LG_0^{l_2}$（l_2=3，5，7，9）到$LG_0^6+LG_0^{l_2}$（l_2=−3，−5，−7，−9）对应的编码为“00000”到“00111”；$LG_0^2+LG_1^{l_2}$（l_2=3，5，7，9）到$LG_0^6+LG_1^{l_2}$（l_2=−3，−5，−7，−9）对应的编码为“01000”到“01111”；$LG_0^2+LG_2^{l_2}$（l_2=3，5，7，9）到$LG_0^6+LG_2^{l_2}$（l_2=−3，−5，−7，−9）对应的编码为“10000”到“10111”；$LG_0^2+LG_3^{l_2}$（l_2=3，5，7，9）到$LG_0^6+LG_3^{l_2}$（l_2=−3，−5，−7，−9）对应的编码为“11000”到“11111”。让编码后的复合涡旋光束依次在自由空间中有序传播，接收端可通过周期渐变光栅的远场衍射光斑图检测出入射光束参数p和l。由于周期渐变光栅只能检测出单束LG涡旋光束的参数，因此需要把图1的32组复合涡旋光束光强图映射转换成对应的32组单束LG涡旋光束光强图，单束LG涡旋光束可以用OAM模态和径向模态的组合表示为$|l,p\rangle$，如图3所示，映射关系为

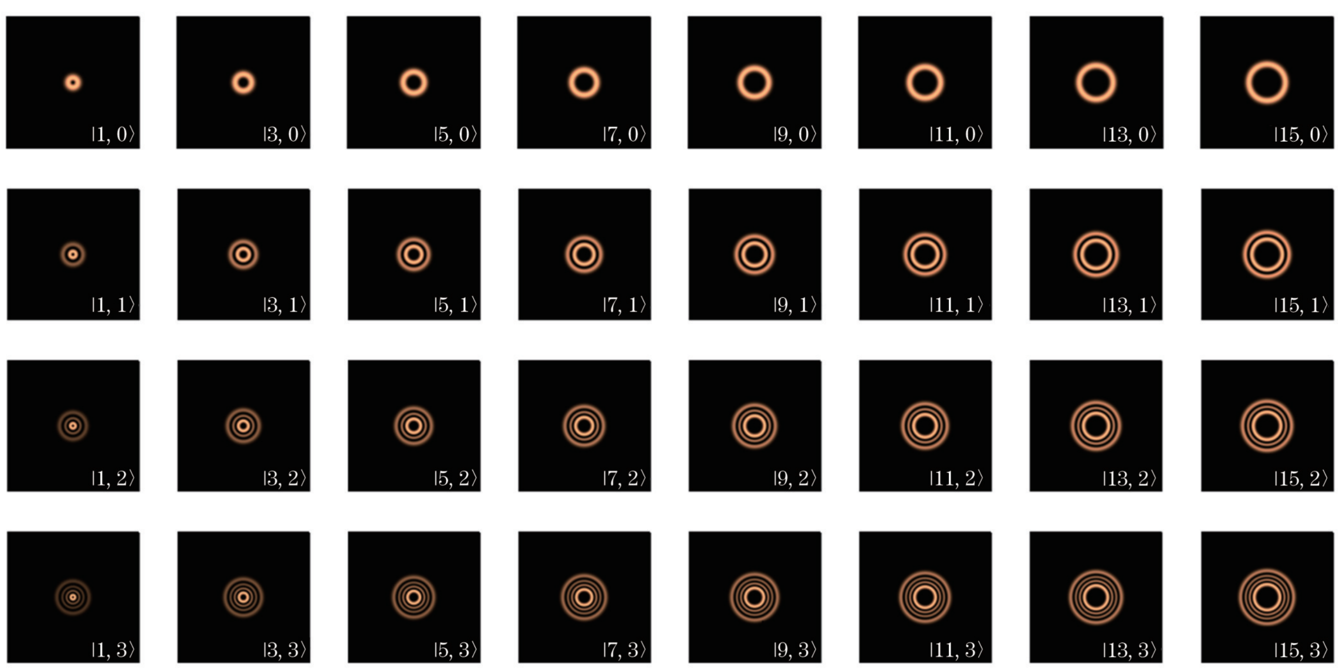

图3　32组复合涡旋光束对应的单束LG涡旋光束光强分布图

Fig. 3　Intensity distributions of single LG vortex beams corresponding to 32 composite vortex beams

$$\mathrm{LG}_{p_1}^{l_1}+\mathrm{LG}_{p_2}^{l_2}\rightarrow\left|\left|l_2-l_1\right|,p=\max(p_1,p_2)\right\rangle=\mathrm{LG}_{\max(p_1,p_2)}^{|l_2-l_1|}。\tag{3}$$

由图 3 可以看出，单束 LG 涡旋光束|1, 0〉到|15, 3〉依次对应复合涡旋光束 $\mathrm{LG}_0^2+\mathrm{LG}_0^3$ 到 $\mathrm{LG}_0^6+\mathrm{LG}_3^{-9}$。例如，单束 LG 涡旋光束|11, 1〉对应复合涡旋光束 $\mathrm{LG}_0^6+\mathrm{LG}_1^{-5}$。

4　周期渐变光栅检测及解码

4.1　周期渐变光栅理论基础

周期渐变光栅是一种振幅型光栅，如图 4 所示，包括两大类，其透过率函数分别为

$$T_1(x,y)=\begin{cases}1,\ \cos\left(\dfrac{2\pi x}{d_0+nx}\right)\geqslant 0\\0,\ \cos\left(\dfrac{2\pi x}{d_0+nx}\right)<0\end{cases},\tag{4}$$

$$T_2(x,y)=\begin{cases}1,\ \cos\left(\dfrac{2\pi x}{d_0+ny}\right)\geqslant 0\\0,\ \cos\left(\dfrac{2\pi x}{d_0+ny}\right)<0\end{cases},\tag{5}$$

式中：d_0 是 $x=0$ 时的光栅常数；n 为周期渐变因子，表示光栅变化的速率。式(4)透过率函数对应的光栅为第一类周期渐变光栅，称为 x 轴方向周期渐变光栅，如图 4(a)所示。式(5)透过率函数对应的光栅为第二类周期渐变光栅，称为 y 轴方向周期渐变光栅，如图 4(b)所示。

当涡旋光束照射周期渐变光栅时，其远场会呈现出与入射涡旋光束阶次相关的衍射场分布。远场衍射可视为多个子光斑按特殊位置排列而成，且相邻子光斑有较暗的节线，节线数目与入射涡旋光束的 OAM 值大小有关，而节线方向与入射涡旋光束 OAM 值的正负有关。通过衍射场的分布情况可检测出入射涡旋光束的径向模态 p 和 OAM 模态 l。

4.2　光束经 x 轴方向周期渐变光栅的检测及解码

对于 x 轴方向周期渐变光栅，当入射 LG 涡旋光束的 l_m 为正时，−1 衍射级的衍射光斑节线方向为左上到右下，+1 衍射级的衍射光斑节线方向为左下到右上；相反，当入射 LG 涡旋光束的 l_m 为负时，−1 衍射级的衍射光斑节线方向为左下到右上，+1 衍射级的衍射光斑节线方向为左上到右下。当入射 LG 涡旋光束 $|l_m=+5,\ 1\rangle$ 照射 x 轴方向周期渐变光栅时，其远场衍射分布如图 5 所示。可见，x 轴方向周期渐变光栅远场衍射光斑的 OAM 模态 l_n 与入射 LG 涡旋光束的 OAM 模态 l_m 满足公式：

$$l_m+l_n=0。\tag{6}$$

由图 5(d)可以看出，+1 衍射级光斑图节线方向为左下到右上，节线个数为 5，则可检测出入射 LG 涡旋光束 OAM 模态 $l_m=+5$。图 5(e)的 0 级衍射光斑图中箭头指的黑圈表示 0 级环数，根据径向模态 $p=0$ 级环数−1，可检测出入射 LG 涡旋光束径向模态 $p=1$。综上可知，入射 LG 涡旋光束为 $|l_m=+5,\ 1\rangle$，则对应的复合涡旋光束为 $\mathrm{LG}_0^2+\mathrm{LG}_1^7$，进而可解码为 01010。最后，将图 3 的 32 组单束 LG 涡旋光束依次经过 x 轴方向周期渐变光栅得到 32 组远场衍射光斑图，如图 6 所示。

4.3　光束经 y 轴方向周期渐变光栅的检测及解码

对于 y 轴方向周期渐变光栅，当入射 LG 涡旋光束的 l_m 为正时，−1 衍射级次的衍射光斑节线为水平方向，+1 衍射级次的衍射光斑节线为竖直方向；同理，当入射 LG 涡旋光束的 l_m 为负时，−1 衍射级次的衍射光斑节线为竖直方向，+1 衍射级次的衍射光斑节线为水平方向。当入射 LG 涡旋光束 $|l_m=+3,2\rangle$ 照射 y 轴方向周期渐变光栅时，其远场衍射分布如图 7 所示。同上，y 轴方向周期渐变光栅远场衍射光斑的 OAM 模态 l_n 与入射 LG 涡旋光束的 OAM 模态 l_m 也满足式(6)。

由图 7(d)可以看出，+1 衍射级光斑图节线为竖直平方向，节线个数为 3，则可检测出入射 LG 涡旋光束 OAM 模态 $l_m=+3$。图 7(e)的 0 级衍射级光斑图中箭头指的黑圈表示 0 级环数，根据径向模态 $p=0$ 级环数−1，可检测出入射 LG 涡旋光束径向模态 $p=2$。综上可知，入射 LG 涡旋光束为 $|l_m=+3,\ 2\rangle$，则对应的复

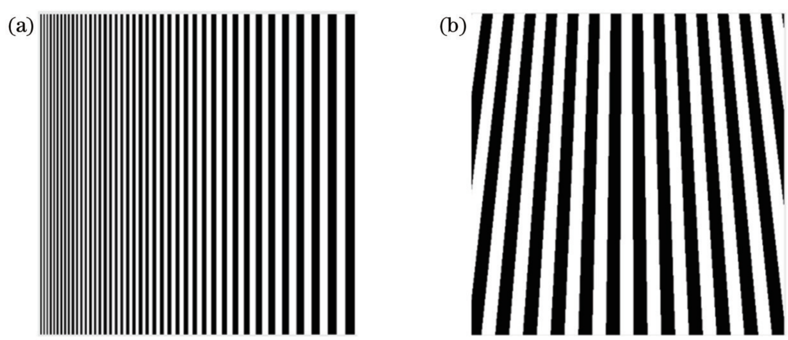

图 4　周期渐变光栅。(a) x 轴方向周期渐变光栅；(b) y 轴方向周期渐变光栅

Fig. 4　Gradually-changing-period gratings. (a) Gradually-changing-period grating in x-axis direction; (b) gradually-changing-period grating in y-axis direction

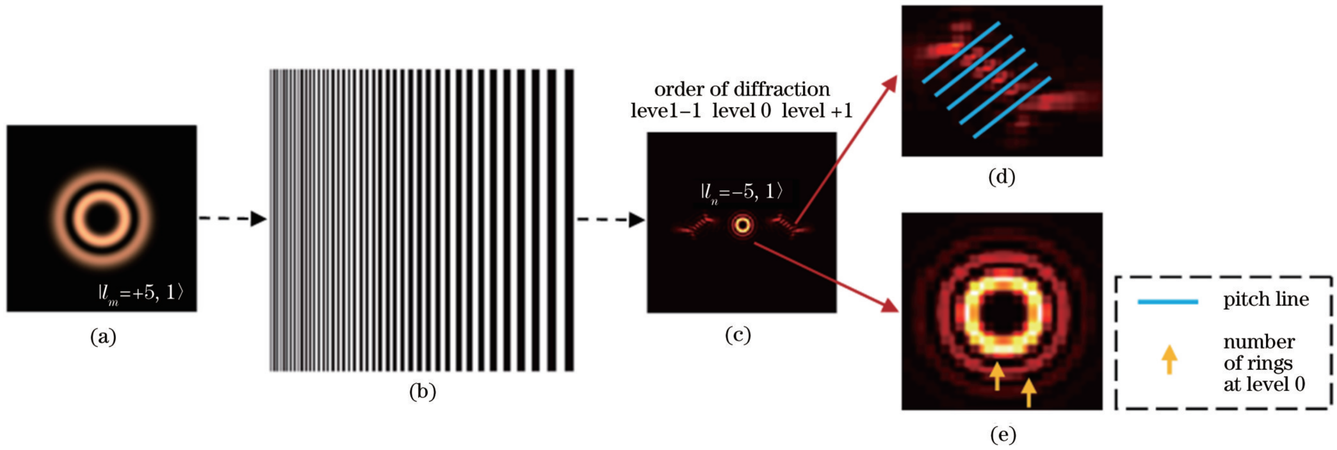

图 5 LG 涡旋光束经过 x 轴方向周期渐变光栅的远场衍射光斑图。(a) LG 涡旋光束 $|l_m=+5, 1\rangle$;(b)沿 x 轴方向的周期渐变光栅;(c)远场衍射光斑图;(d)+1 级衍射光斑图;(e) 0 级衍射光斑图

Fig. 5 Far-field diffraction pattern of LG vortex beam passing through gradually-changing-period grating in x-axis direction. (a) LG vortex beam $|l_m=+5, 1\rangle$; (b) gradually-changing-period grating along x-axis; (c) far-field diffraction pattern; (d) +1 order diffraction pattern; (e) 0 order diffraction pattern

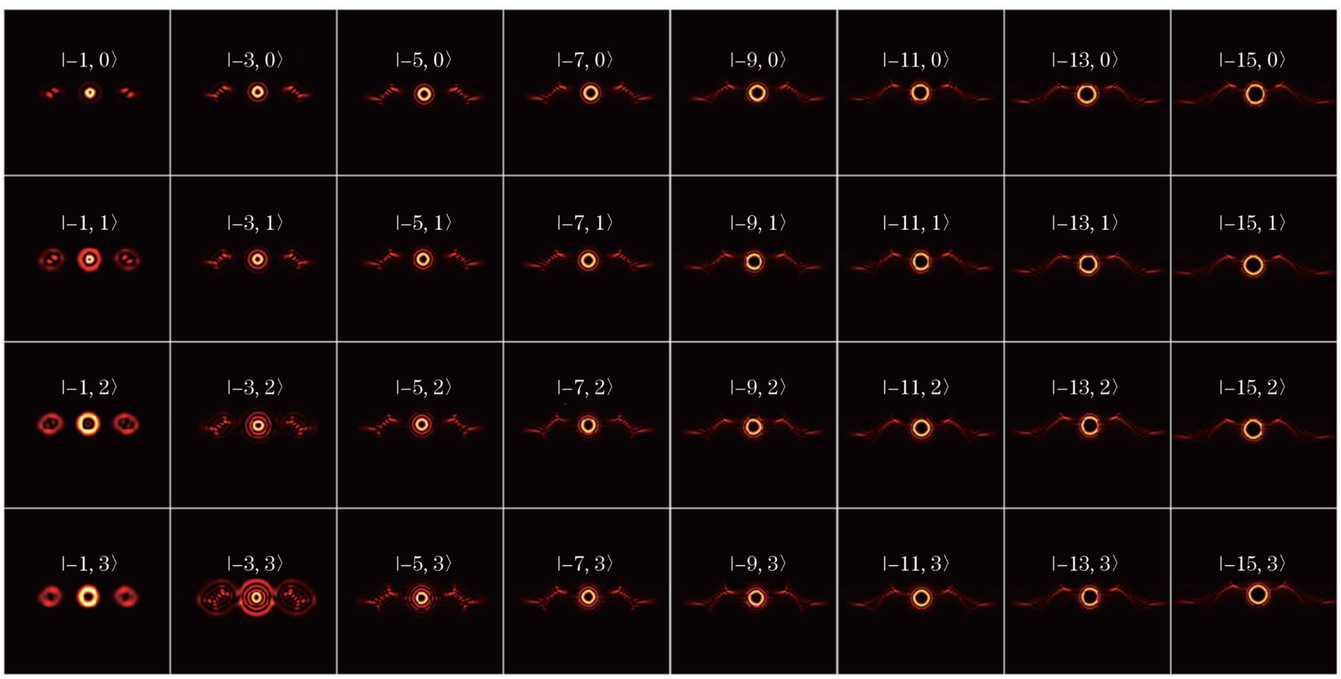

图 6 32 组单束 LG 涡旋光束经过 x 轴方向周期渐变光栅所对应的远场衍射光斑图

Fig. 6 Far-field diffraction patterns corresponding to 32 single LG vortex beams passing through gradually-changing-period grating in x-axis direction

合涡旋光束为 $LG_0^2+LG_2^5$,进而可解码为 10001。最后,将图 3 的 32 组单束 LG 涡旋光束依次经过 y 轴方向周期渐变光栅得到 32 组远场衍射光斑图,如图 8 所示。

5 结　论

基于理论推导和数值模拟,本文得到了一束具有固定 OAM 模态和径向模态的 LG 涡旋光束与另一束具有 8 种相同间隔的 OAM 模态($l=\pm3, \pm5, \pm7, \pm9$)和 4 种径向模态($p=0, 1, 2, 3$)的 LG 涡旋光束共轴叠加产生的 32 组复合涡旋光束光强分布图,并使用 5 位二进制序列对其依次进行编码,随后采用提出的周期渐变光栅进行检测并解码。研究结果表明,随着 OAM 模态和径向模态的增加,提出的 x、y 轴方向周期渐变光栅均能检测出单束 LG 涡旋光束的参数 p 和 l,且不受光强图各环半径和环数增加的影响。最终,根据检测的结果可推算出对应的复合涡旋光束并正确解码。该研究成果为拓展 OAM 模态在信息编/解码领域的应用提供了一定的理论基础。

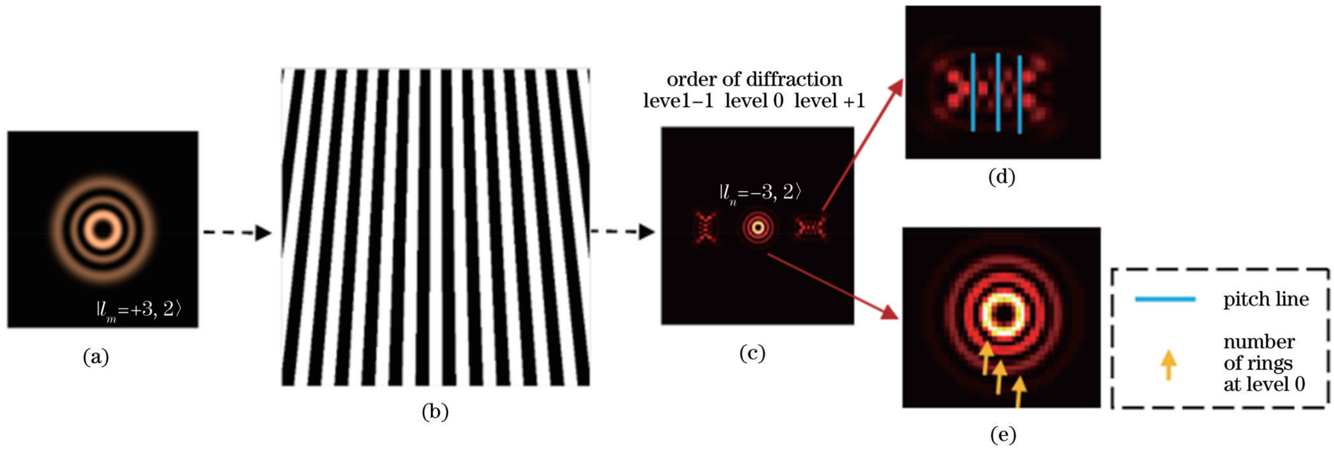

图 7 LG 涡旋光束经过 y 轴方向周期渐变光栅的远场衍射光斑图。(a) LG 涡旋光束 $|l_m=+3,2\rangle$；(b)沿 y 轴方向的周期渐变光栅；(c)远场衍射光斑图；(d) +1 级衍射光斑图；(e) 0 级衍射光斑图

Fig. 7 Far-field diffraction pattern of LG vortex beam passing through gradually-changing-period grating in y-axis direction. (a) LG vortex beam $|l_m=+3, 2\rangle$; (b) gradually-changing-period grating along y-axis; (c) far-field diffraction pattern; (d) +1 order diffraction pattern; (e) 0 order diffraction pattern

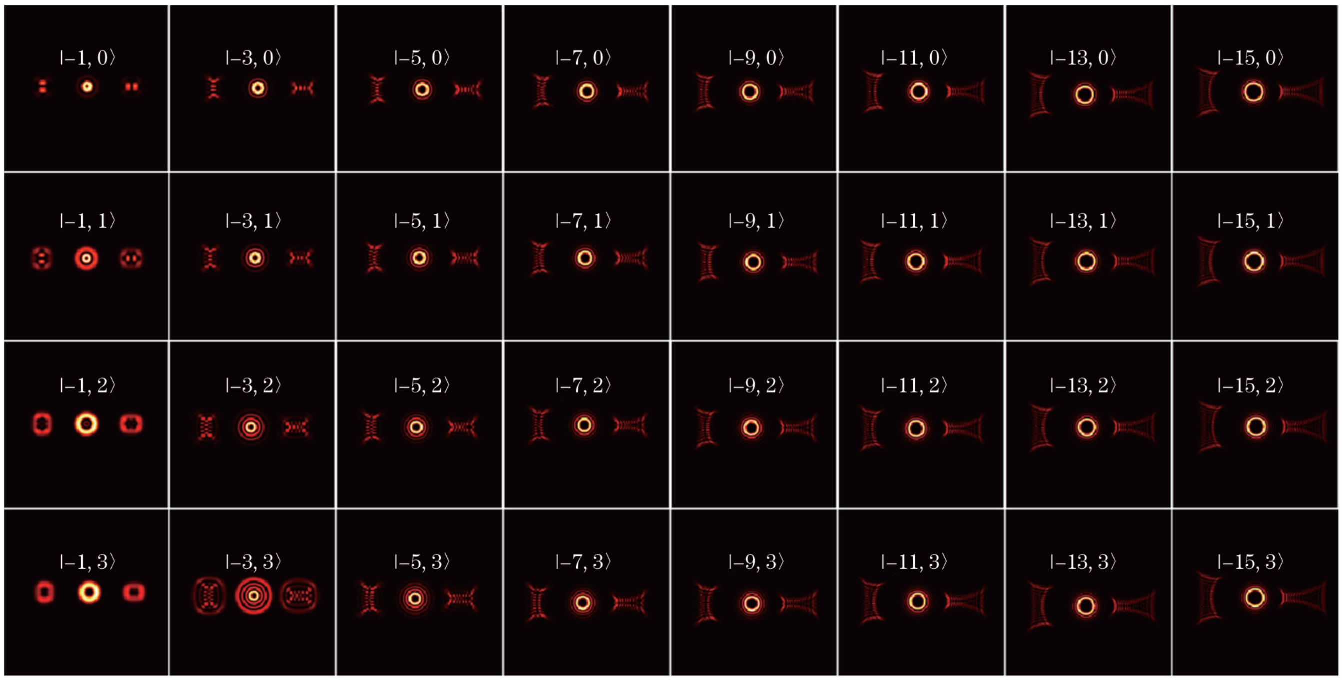

图 8 32 组单束涡旋光束经过 y 轴方向周期渐变光栅所对应的远场衍射光斑图

Fig. 8 Far-field diffraction patterns corresponding to 32 single LG vortex beams passing through gradually-changing-period grating in y-axis direction

参 考 文 献

[1] Wang J, Liu J, Li S H, et al. Orbital angular momentum and beyond in free-space optical communications[J]. Nanophotonics, 2022, 11(4): 645-680.

[2] Li M M, Yan S H, Liang Y S, et al. Transverse spinning of particles in highly focused vector vortex beams[J]. Physical Review A, 2017, 95(5): 053802.

[3] Avramov-Zamurovic S, Nelson C. Experimental study: underwater propagation of polarized flat top partially coherent laser beams with a varying degree of spatial coherence[J]. Optics Communications, 2018, 424: 54-62.

[4] Allen L, Beijersbergen M W, Spreeuw R J, et al. Orbital angular momentum of light and the transformation of Laguerre-Gaussian laser modes[J]. Physical Review A, 1992, 45(11): 8185-8189.

[5] Willner A E, Huang H, Yan Y, et al. Optical communications using orbital angular momentum beams[J]. Advances in Optics and Photonics, 2015, 7(1): 66-106.

[6] Krenn M, Handsteiner J, Fink M, et al. Twisted photon entanglement through turbulent air across Vienna[J]. Proceedings of the National Academy of Sciences of the United States of America, 2015, 112(46): 14197-14201.

[7] Nicolas A, Veissier L, Giner L, et al. A quantum memory for orbital angular momentum photonic qubits[J]. Nature Photonics,

2014, 8(3): 234-238.

[8] Grier D G. A revolution in optical manipulation[J]. Nature, 2003, 424(6950): 810-816.

[9] Meier M, Romano V, Feurer T. Material processing with pulsed radially and azimuthally polarized laser radiation[J]. Applied Physics A, 2007, 86(3): 329-334.

[10] Tamburini F, Thidé B, Molina-Terriza G, et al. Twisting of light around rotating black holes[J]. Nature Physics, 2011, 7(3): 195-197.

[11] Qin Y, Yang H J, Jiang P, et al. Research for propagation properties of LG beam through Cassegrain antenna system in a turbulent atmosphere[J]. Optics Express, 2020, 28(10): 14436-14447.

[12] Volke-Sepulveda K, Garcés-Chávez V, Chávez-Cerda S, et al. Orbital angular momentum of a high-order Bessel light beam[J]. Journal of Optics B: Quantum and Semiclassical Optics, 2002, 4(2): S82-S89.

[13] 何德, 闫红卫, 吕百达. 厄米-高斯涡旋光束形成的合成光涡旋及演化[J]. 中国激光, 2009, 36(8): 2023-2029.
He D, Yan H W, Lü B D. Evolution and composite optical vortices of Hermite-Gaussian vortex beams[J]. Chinese Journal of Lasers, 2009, 36(8): 2023-2029.

[14] 王明军, 余文辉, 黄朝军. 水下拉盖尔-高斯涡旋光束及其叠加态传输特性的实验研究[J]. 光学学报, 2023, 43(6): 0626001.
Wang M J, Yu W H, Huang C J. Experimental study on the transmission characteristics of underwater Laguerre-Gaussian vortex beam and its superposition state[J]. Acta Optica Sinica, 2023, 43(6): 0626001.

[15] Anguita J A, Herreros J, Djordjevic I B. Coherent multimode OAM superpositions for multidimensional modulation[J]. IEEE Photonics Journal, 2014, 6(2): 7900811.

[16] 贺超, 叶卉, 陈田, 等. 基于光学亮环晶格的空间光编码通信[J]. 光学学报, 2020, 40(11): 1106002.
He C, Ye H, Chen T, et al. Space optical encoding communication based on optical bright-ring lattice[J]. Acta Optica Sinica, 2020, 40(11): 1106002.

[17] 南久航, 韩一平. 双路多进制涡旋光通信[J]. 光学学报, 2021, 41(12): 1206001.
Nan J H, Han Y P. Dual-channel multiband vortex optical communication[J]. Acta Optica Sinica, 2021, 41(12): 1206001.

[18] Wang X H, Song Y X, Pang F F, et al. High-dimension data coding and decoding by radial mode and orbital angular momentum mode of a vortex beam in free space[J]. Optics and Lasers in Engineering, 2021, 137: 106352.

[19] Volke-Sepúlveda K, Santillán A O, Boullosa R R. Transfer of angular momentum to matter from acoustical vortices in free space[J]. Physical Review Letters, 2008, 100(2): 024302.

[20] Emile O, Emile J. Young's double-slit interference pattern from a twisted beam[J]. Applied Physics B, 2014, 117(1): 487-491.

[21] Zheng S, Wang J. Measuring orbital angular momentum (OAM) states of vortex beams with annular gratings[J]. Scientific Reports, 2017, 7(1): 1-9.

[22] Gibson G, Courtial J, Padgett M J, et al. Free-space information transfer using light beams carrying orbital angular momentum[J]. Optics Express, 2004, 12(22): 5448-5456.

[23] Zhang N, Yuan X C, Burge R E. Extending the detection range of optical vortices by Dammann vortex gratings[J]. Optics Letters, 2010, 35(20): 3495-3497.

[24] Sztul H I, Alfano R R. Double-slit interference with Laguerre-Gaussian beams[J]. Optics Letters, 2006, 31(7): 999-1001.

[25] Fu S Y, Wang T L, Zhang S K, et al. Integrating 5×5 Dammann gratings to detect orbital angular momentum states of beams with the range of −24 to +24[J]. Applied Optics, 2016, 55(7): 1514-1517.

[26] Bai Y H, Lv H R, Fu X, et al. Vortex beam: generation and detection of orbital angular momentum[J]. Chinese Optics Letters, 2022, 20(1): 012601.

[27] Wang P P, Xiong W J, Huang Z B, et al. Orbital angular momentum mode logical operation using optical diffractive neural network[J]. Photonics Research, 2021, 9(10): 2116-2124.

[28] Fang J C, Li J P, Kong A R, et al. Optical orbital angular momentum multiplexing communication via inversely-designed multiphase plane light conversion[J]. Photonics Research, 2022, 10(9): 2015-2023.

[29] Anguita J A, Neifeld M A, Vasic B V. Turbulence-induced channel crosstalk in an orbital angular momentum-multiplexed free-space optical link[J]. Applied Optics, 2008, 47(13): 2414-2429.

Encoding/Decoding of Composite Vortex Beams with Spaced Orbital Angular Momentums

Wu Pengfei[1*], Wang Xiaodie[1], Wang Jiao[2], Tan Zhenkun[3], Jia Zhiyuan[1]

[1]*School of Automation and Information Engineering, Xi'an University of Technology, Xi'an* 710048, *Shaanxi, China*;

[2]*School of Electronic Information and Artificial Intelligence, Shaanxi University of Science & Technology, Xi'an* 710021, *Shaanxi, China*;

[3]*School of Opto-electronical Engineering, Xi'an Technological University, Xi'an* 710021, *Shaanxi, China*

Abstract

Objective With the advantages of high flexibility, high security, and large communication bandwidths, vortex beams play an important role in many fields, such as quantum entanglement, spatial optical communications, particle manipulation, and optical microscopy. In optical communication applications, the orbital angular momentums (OAMs) of vortex beams can be used as a new encoding method for high-dimensional information encoding. This method can not only achieve mode-division multiplexing and scale the capacity of optical communications but also improve the channel capacity and spectral efficiency of optical communications. It thus provides a potential solution for future high-speed, high-capacity, and high-spectral-efficiency optical communication technologies. This study proposes an encoding method based on OAM and radial modes for composite vortex beams. It uses a 5-bit binary sequence to encode the light intensity distributions of 32 different composite vortex beams generated by the coaxial superposition of two vortex beams. The topological charge and radial index of the incident vortex beam are detected by the proposed gradually-changing-period gratings for decoding purposes. The research results of this study provide a theoretical basis for extending the applications of the OAM modes of vortex beams in the encoding and decoding field.

Methods To generate large topological charges and make demodulation easier, this study proposes an optical communication method and system featuring the encoding of composite vortex beams with spaced OAM modes. Specifically, a Laguerre-Gaussian (LG) vortex beam with fixed OAM and radial modes is coaxially superposed with an LG vortex beam with four radial modes ($p=0$, 1, 2, 3) and eight equally spaced OAM modes ($l=\pm 3$, ± 5, ± 7, ± 9) to generate and further encode the light intensity distributions of 32 different composite vortex beams with a 5-bit binary sequence. Then, Eq. (3) is used to convert the 32 composite vortex beams into 32 single LG vortex beams, which will irradiate the proposed gradually-changing-period gratings in the x-axis and y-axis directions. The p and l of the single LG vortex beams can be successfully detected by leveraging the far-field diffraction patterns of the gratings and then be used to derive the composite vortex beams. In this way, the information can be decoded correctly.

Results and Discussions The light intensity distributions of the 32 composite vortex beams are shown in Fig. 1. The results reveal multi-ring patterns in the light intensity distributions. The radius of each ring increases as the OAM mode $|l_2|$ rises, and the number of patterns in each ring is $|l_2-l_1|$. In addition, the number of rings in the light intensity distributions increases with the radial mode p_2, and the number of rings is $p=\max(p_1, p_2)+1$. Figure 2 presents the encoding sequences for the composite vortex beams shown in Fig. 1. According to Fig. 2, the corresponding encoding sequences for the composite vortex beams $LG_0^2+LG_0^3$ - $LG_0^6+LG_3^{-9}$ are 00000-11111. Figure 3 illustrates the light intensity distributions of the 32 single LG vortex beams converted by Eq. (3) from the composite vortex beams shown in Fig. 1. In Fig. 3, the OAM value of a single LG vortex beam is the absolute value of the difference between the OAM values of the two superposed beams, and the radial mode of a single LG vortex beam is the maximum value of the radial modes of the two superposed beams. Figures 4(a) and 4(b) are the proposed gradually-changing-period gratings in the x-axis and y-axis directions, respectively. Figure 4 indicates that the period changes gradually in the x-axis and y-axis directions, respectively. A comparison between Figs. 5 and 7 suggests that when the beam passes through a gradually-changing-period grating, its adjacent far-field diffraction sub-pattern has dark nodal lines. The number of the nodal lines is related to the OAM value of the incident LG vortex beam and satisfies Eq. (6). Moreover, the direction of the nodal lines is determined by whether the OAM value of the incident LG vortex beam is positive or negative. Regarding the x-axis gradually-changing-period grating, the nodal lines of the diffraction pattern at the -1 diffraction order are from upper left to lower right while those of the diffraction pattern at the $+1$ diffraction order are from lower left to upper right when the l_m of the incident vortex beam is positive. In the case of the y-axis gradually-changing-period grating, the nodal lines of the diffraction pattern at the -1 diffraction order are horizontal while those of the diffraction pattern at the $+1$ diffraction order are vertical when the l_m of the incident vortex beam is positive. Figures 6 and 8 show the 32 far-field diffraction patterns produced after the 32 single LG vortex beams pass through the x-axis and y-axis gratings, respectively. The results suggest that the far-field diffraction patterns can be used to successfully detect the parameters of the single LG vortex beams for correct decoding without being affected by the increases in the OAM or radial modes.

Conclusions This study derives the expression of the intensity of each composite vortex beam generated by the coaxial superposition of two LG vortex beams and uses a 5-bit binary sequence to encode the simulated light intensity distributions of 32 different composite vortex beams. The far-field diffraction patterns of the x-axis and y-axis gradually-changing-period gratings designed and proposed in this study can be used to successfully detect the parameters p and l of the single LG vortex beams. The results show that a multi-ring pattern can be observed in the light intensity distributions. The number of rings is $p=\max(p_1, p_2)+1$, and the number of patterns in each ring is $|l_2-l_1|$. In addition, the proposed x-axis and y-axis gradually-changing-period gratings can be utilized to successfully detect the parameters of the incident beams for correct decoding without being affected by the radius of each ring or the number of rings in the light intensity distributions.

Key words physical optics; composite vortex beam; orbital angular momentum; radial mode; gradually-changing-period grating; far-field diffraction pattern